SolarPACES 2024, 30th International Conference on Concentrating Solar Power, Thermal, and Chemical Energy Systems

CSP Integration, Markets, and Policy

https://doi.org/10.52825/solarpaces.v3i.2506

Published: 22 Sep. 2025

Materials Comparison for Reducing Heliostats Production Costs

Javier A. Martell[1,*], Kenneth M. Armijo[1], and Dimitri A. Madden[1]

[1]Sandia National Laboratories, USA

*Correspondence: Javier A. Martell, jamarte@sandia.gov

Abstract. The alarming issue of climate change and the necessity to increase the renewable energy stake has become the driving force for cost reduction measures taken in various renewable technologies. Concentrated Solar Power (CSP) is an increasingly attractive solar energy technology that uses heliostats to provide controllable, rapid heating and thermal energy storage (TES) benefits, which can use high temperature fluids (HTF) for higher efficiencies. The cost of installation for a commercial heliostat assuming a production volume of 22,239 heliostats, which represents a solar field aperture area of 1,078,592 m^2, is \$127/m^2, or 136.98 million for the solar field [1]. Around 31% of the cost comes from manufactured parts which include the heavy use of steel, which can be subject to high price volatility, to ensure structural stability under wind load conditions. By studying the structural vibration response for different types of composite materials, a case can be made to switch from the heavy use of galvanized steel to a hybrid or even complete use of composite materials for heliostat construction. This paper presents a structural vibration response comparison between Steel AISI 1020, Glass Fiber Reinforced Polymer (S-Glass and E-Glass), Basalt Fiber Reinforced Polymer, and Carbon Fiber Reinforced Polymer (230, 290, and 395 GPa.) for heliostats structure manufacturing.

Keywords: Heliostats, Cost Reduction, Composite Materials

1. Introduction

Global energy-related CO_2 emissions grew by 1.1% in 2023, increasing 410 million tones (Mt) to reach a new record high of 37.4 billion tones (Gt). This compares with an increase of 490 Mt in 2022 (1.3%). Emissions from coal accounted for more than 65% of the increase in 2023 [2]. This alarming issue increases the necessity for renewable energy stake and cost reduction methods for renewable technologies. CSP has received significant attention among researchers, power-producing companies, and state policymakers for its bulk electricity generation capability, overcoming the intermittency of solar resources [3]. The challenge, as with most renewable energies, is the cost. Currently, the levelized cost of electricity (LCOE) for CSP is 7.6 cents per kWh. To improve CSP adoption by lowering the cost of resilient heliostats, lower structural costs need to be realized which also can provide adequate operational strength from high wind loads need to be minimized. A large percentage (up to 40%) of the cost of CSP plants comes from manufacturing costs of heliostats (section 1.1 presents a cost update for heliostats). Heliostats are exposed to a natural environment where high wind loads can cause structural failures and affect the optical performance of heliostats. The mirror support structure is also one of the major cost drivers of the heliostats for both large and small heliostats. Therefore, to reduce the cost of the heliostats, it is important to accurately estimate the static and dynamic wind loads so that the designed wind load can be reduced and optimize the structure [4]. In this paper, a digital vibrational response study of a heliostat structure at varying wind

speeds, and the heliostat made of varying manufacturing materials, is presented to reduce the overall costs of heliostats.

1.1 Heliostats Cost Update

In 2022, the National Renewable Energy Laboratory (NREL) conducted an assessment on current heliostat manufacturing costs. This research team performed a detailed bottom-up manufacturing cost estimate for two heliostat designs: (1) a commercial design, the Stellio and (2) an advanced/developing heliostat design, the SunRing. For both designs, the bottom-up manufacturing cost estimates included all components for manufacturing and assembly in a manufacturing facility (e.g., struts and frame) using Design for Manufacturing and Assembly (DFMA) software, and the purchased parts (e.g., mirrors, control systems, and drives). The field-assembly and construction activities were also considered to determine the installed cost of the modeled solar fields. In both cases, the modeled heliostat field area was approximately 1.1 million square meters (Mm^2) in total solar field aperture area, which is the solar field area needed for a CSP baseload power tower plant. This modeled ~1.1 Mm^2 solar field is suited for an 80- MWe CSP power tower plant with 12–16 hours (hrs.) of thermal energy storage based on system advisor model (SAM) analysis. The land area for the modeling was approximately 1 square mile. For the Stellio solar field of 1,078,592 m^2 that was comprised of 22,239 heliostats, the estimated installed cost was \$127/m^2. The installed cost included the manufacturing cost, the purchased components, and installation. The SunRing analysis estimated the installed cost of 40,000 heliostats with 1,078,560 m^2 of aperture area to be approximately \$96/m2 [1]. Figure 1 shows the cost breakdown for the heliostats. #

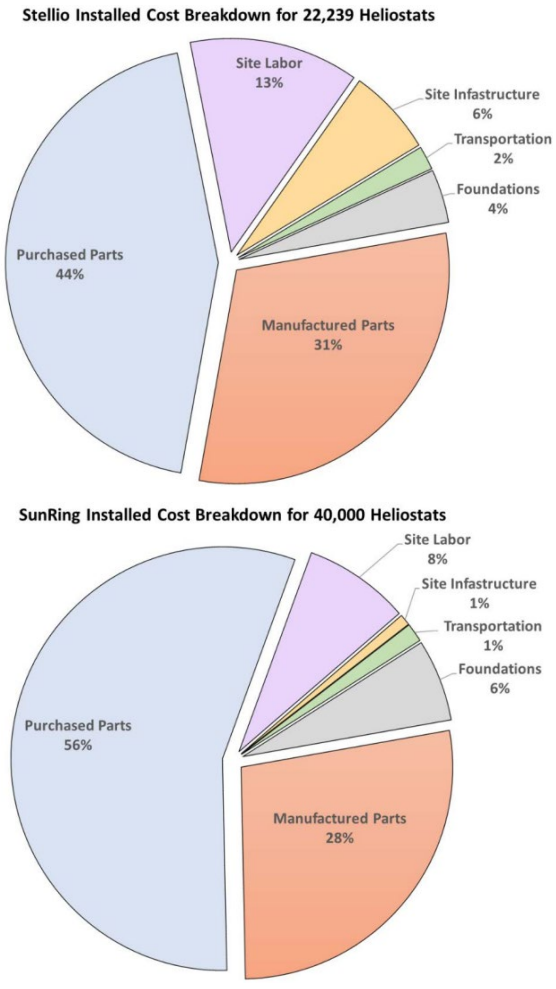

Figure 1. *Cost breakdown for Stellio (up) and SunRing (down) heliostats [1].*

2. Methods

2.1 CFD Wind Tunnel Model

The Australian Solar Thermal Research Initiative (ASTRI) provided Sandia National Laboratories (SNL) with a heliostat structure computer aided design (CAD) file that was assessed as an exemplar for next generation heliostat materials optimization. This heliostat structure was used for a vibrations analysis. The complete CAD file utilized several components to make a complete assembly file. This assembly file could not be imported directly to Ansys because of its complexity and number of contacts. Because of this, a simplified single part file was created from the assembly to reduce the number of contacts and overall complexity of the model to import to an ANSYS Fluent modelling environment. The assembly and simplified part file can be seen in figure 1.

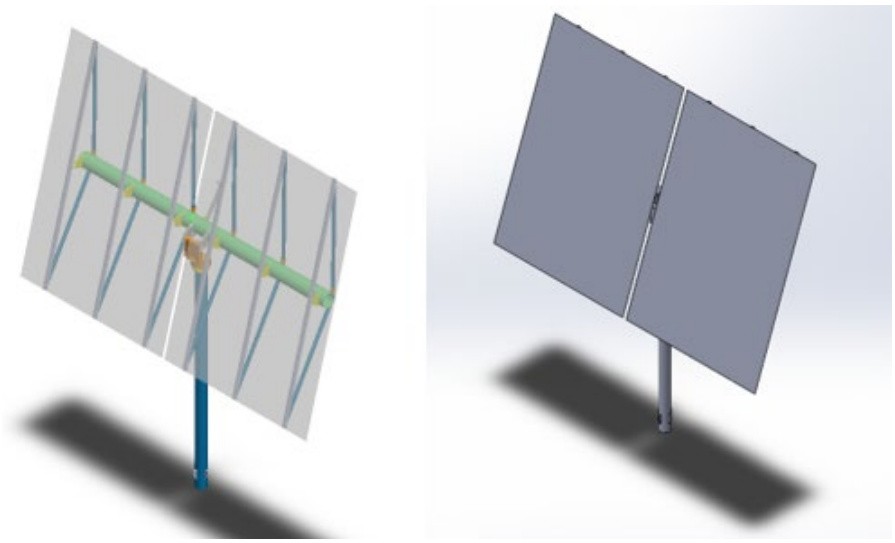

Figure 2. *Isometric view of ASTRI full heliostat assembly (left) and simplified part file (right).*

To capture wind loading effects on the structure, a digital wind tunnel was created using Ansys Fluent to simulate the wind hitting the structure. First, a rectangular enclosure is created around the heliostat CAD model. This enclosure will serve as the fluid domain for the air. The dimensions of the enclosure were defined based on some general guidelines. The length of the enclosure upstream of the model (inlet) should be sufficient to develop a uniform and fully developed flow before it reaches the model (5-10 times the characteristic length). The downstream length (outlet) is important to allow the wake and flow disturbances to dissipate without affecting the results near the model (10-15 times the characteristic length). The lateral and vertical boundaries of the wind tunnel enclosure should be placed far enough from the model to avoid interference with the flow (5-10 times the characteristic length). The characteristic length refers to the length or diameter of the model. The characteristic length of the model is 6.64 m. With this, the lengths of the enclosure are calculated to be 46.48, 99.6, and 33.2 m. for the inlet, outlet, and sides respectively. A Body of Influence (BOI) is also created by enclosing the region close to the heliostat and extending it to the outlet. The BOI is needed to have a refined mesh around the model for accurate results. Figure 2 shows the enclosure and the BOI around the model.

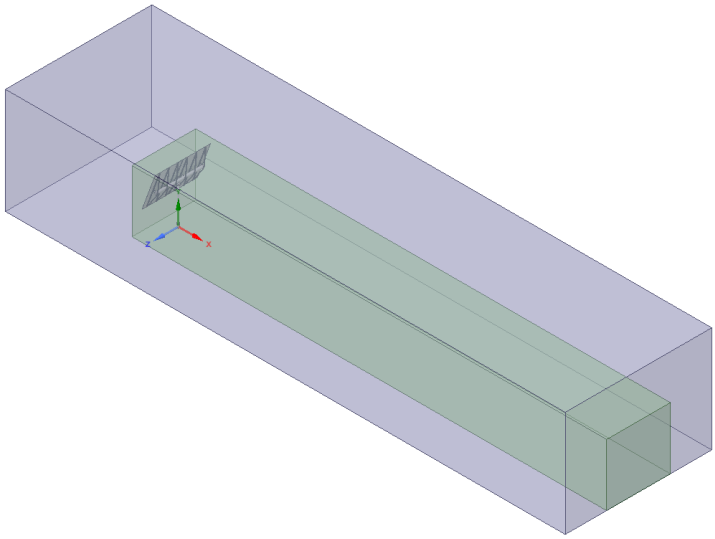

Figure 3. *Isometric view of enclosure (purple) and BOI (green0 around the heliostat model.*

A poly-hexcore mesh was created by specifying two local sizing. One in the heliostat of 0.01 m. size, and one on the BOI of 0.1 m. size. The global min and max size for the model are 0.5 and 1 m respectively. Boundary layers were added between the heliostat faces, and the BOI. The model consists of a total of ~2,000,000 elements. Figure 3 shows the volume mesh of the model.

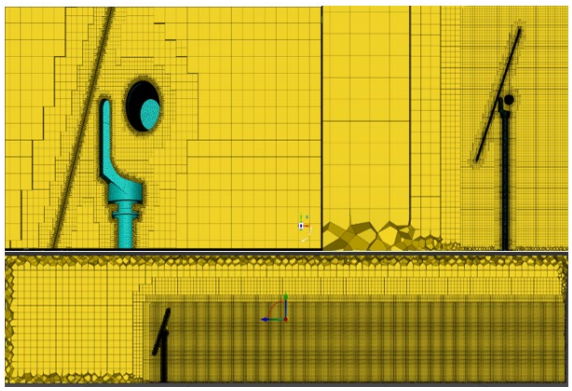

Figure 4. *Cross-section view of volume mesh.*

The model uses steady state k-omega turbulence model. Air velocities of 4, 8, and 16 m/s normal to the inlet were specified in the model. Velocity vectors can be seen in figure 4. The static pressure data, shown in figure 5, on the heliostat walls was exported from Fluent along with its x, y, and z directions to be used as load data in the FEA analysis.

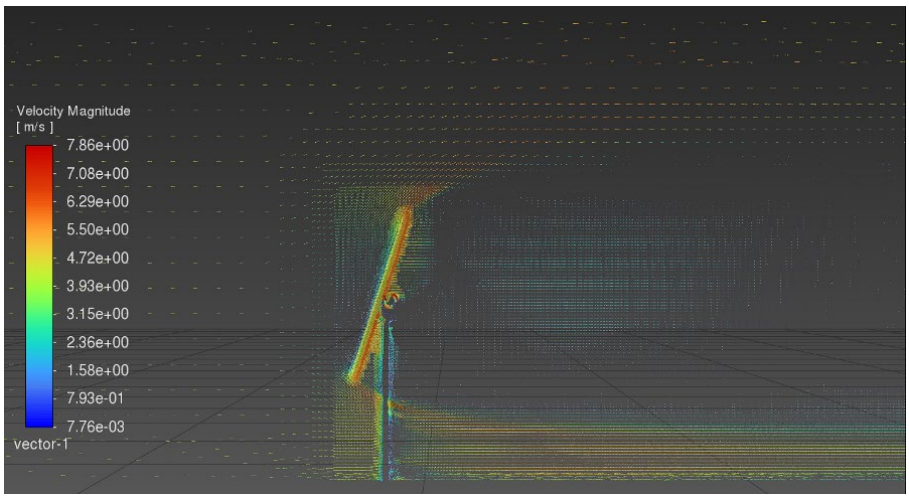

Figure 5. *Cross-section view of velocity magnitude vector.*

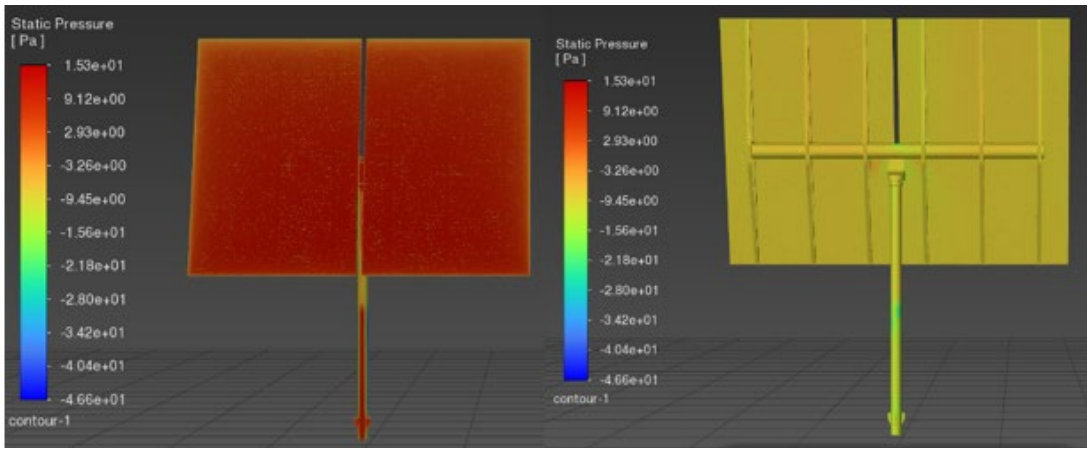

Figure 6. *Front (left) and back (right) view of static pressure contour.*

2.2 FEA Mode Superposition Harmonic Analysis

The harmonic response analysis determines the steady-state response of a structure that is subjected to loads that vary sinusoidally over time. This analysis is used to verify whether the designs will successfully handle resonance, fatigue, and other harmful effects of forced vibrations. The mode superstition method adds up factored mode shapes from a modal analysis to calculate the structures response.

Seven materials are used for the structure in this study. Steel-AISI1020, Glass Fiber Reinforced Polymer (S-Glass and E-Glass), Basalt Fiber Reinforced Polymer (BFRP), and Carbon Fiber (CF 230, 290, and 395). Glass is also used as the material for the heliostat panels. Table 1 shows the material properties for each one.

Table 1. *Material properties for heliostat vibration response study.*

Materials	Density (kg/m^3)	Young's Modulus (GPa)	Poisson's Ratio	Bulk Modulus (GPa)	Shear Modulus (GPa)	Damping Coefficient
Steel-A-ISI1020	7870	205	0.29	162.7	794.57	0.03 [5]
S-Glass	2500	90	0.22	53.57	36.88	0.0429 [6]
E-Glass	2600	73	0.22	43.45	29.91	0.0242 [7]
BFRP	2800	89	0.30	74.16	34.23	0.018
CF 230	1800	230	0.26	-	9	0.0162 [8]
CF 290	1800	290	0.26	-	9	0.0162 [8]
CF 395	1800	395	0.26	-	8	0.0162 [8]
Glass	2500	70	0.22	41.66	28.68	-

A modal analysis is performed to determine the natural frequencies of the structure. The natural frequencies are the frequencies at which a structure naturally tends to vibrate when disturbed. These frequencies are important to understand since any resonance that matches this frequency can cause structural failure. The natural frequencies will depend on the material and a fix location. Each material was specified, and its natural frequencies found. The bottom face of the post was specified as the fix location of the system. Figure 6 shows the model global axis. Sixty modes were specified for the solver to find. The number of modes to find will depend on the total effective mass for each direction. It is recommended that the total effective mass at the direction in which the forces are applied is above 0.80. In this case, sixty modes were enough to reach this total effective mass. The displacement contour for the first four modes is shown in figure 7.

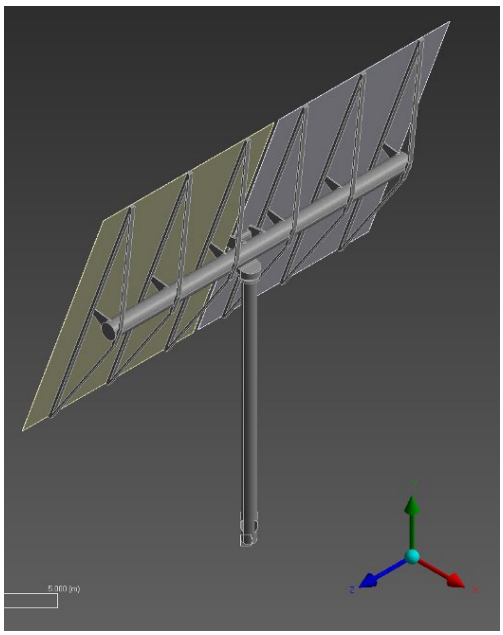

Figure 7. *Isometric view of model global axis.*

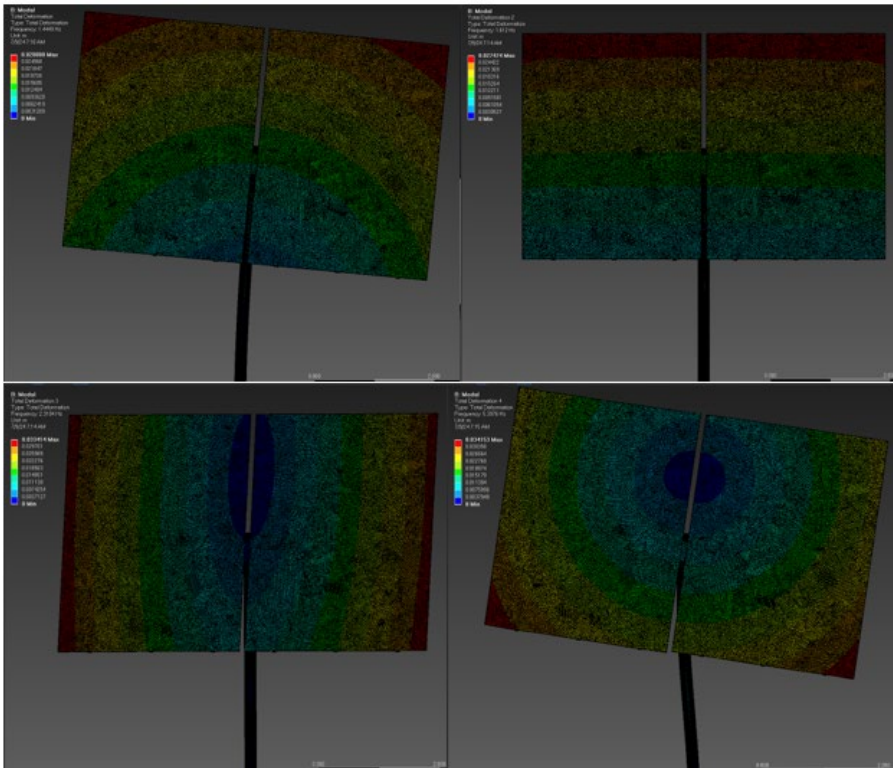

Figure 8. *Displacement contour of normal modes at 1.449, 1.612, 2.3104, and 5.3976 Hz.*

By utilizing the normal modes frequency range (0.5 – 33 Hz.), importing the pressure load for each wind speed from Fluent, and specifying the damping coefficient for each material, a harmonic analysis study is made to extract the vibration response of the structure. Figure 7 shows the imported pressure load contour on the structure.

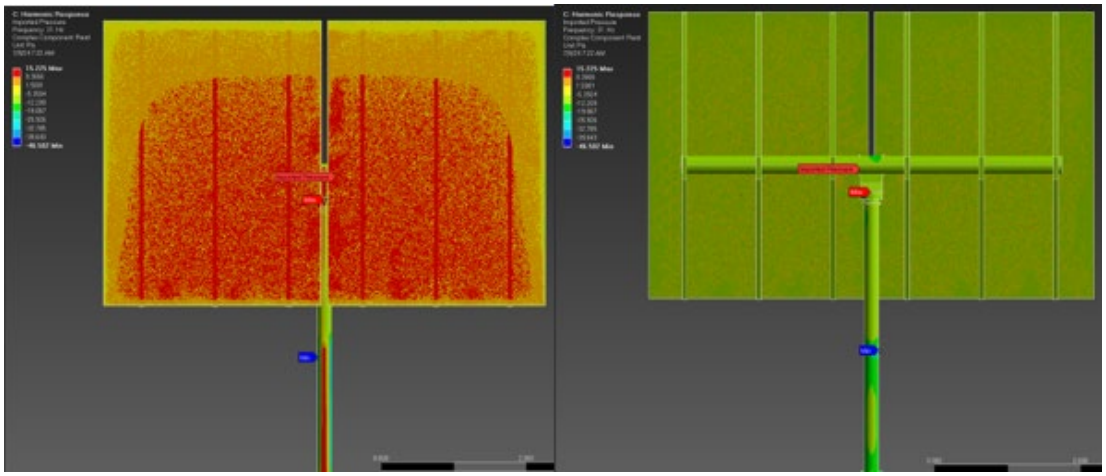

Figure 9. *Front (left) and back (right) view of imported pressure load contour.*

3. Results and Discussion

All materials were studied at 4, 8, and 16 m/s wind velocities. The frequency response for directional deformation and normal stresses in x, y, and z directions were plotted and the data for the maximum directional deformation and normal stresses were used to acquire maximum total deformation and Von Misses stresses. Since the direction of the wind hitting the structure

was constant, in all cases the maximum directional deformation occurred in the x-direction, and the maximum normal stress occurred in the y-direction. Table 2 shows the maximum directional deformation and normal stress for all materials at all wind speeds. The carbon fiber experienced the most deformation from all the materials, but the normal stress stayed at anormal range. The BFRP and the E-Glass experiences similar deformation and stresses. The steel experienced the least deformation from all the materials, but at higher wind speeds, the stresses increased. The S-Glass deformed more than the steel, but the stresses experienced were the lowest from all materials.

Table 2. *Materials maximum directional deformation and normal stresses at 4, 8, and 16 m/s wind speeds.*

Material	**4 m/s**		**8 m/s**		**16 m/s**	
	Max Directional Deformation (m)	**Max Normal Stress (MPa)**	**Max Directional Deformation (m)**	**Max Normal Stress (MPa)**	**Max Directional Deformation (m)**	**Max Normal Stress (MPa)**
Steel-A-ISI1020	0.00214	0.024778	0.00856	0.099108	0.0342	0.396230
S-Glass	0.00402	0.013243	0.0161	0.052963	0.0659	0.218720
E-Glass	0.00440	0.025003	0.0176	0.100020	0.0704	0.399920
BFRP	0.00409	0.029915	0.0164	0.119670	0.0654	0.478460
CF 230	0.0104	0.023469	0.0416	0.093872	0.16642	0.375430
CF 290	0.0104	0.022453	0.0416	0.089804	0.16649	0.359160
CF 395	0.0146	0.015680	0.0583	0.062525	0.23298	0.249730

The total deformation and Von Misses stresses can be acquired by specifying the frequency at which the maximum directional deformation and normal stresses occurred. For the S-Glass, at 16 m/s wind speeds, the frequencies for the maximum directional deformation and normal stresses are 2.316 and 23.26 Hz respectively. Figure 9 shows the total deformation, and figure 10 the Von Misses stresses. The total deformation shows the structure oscillating back and forth which agrees with the wind hitting the structure directly. The Von Misses stress shows the maximum stress occurring at the back support of the heliostat.

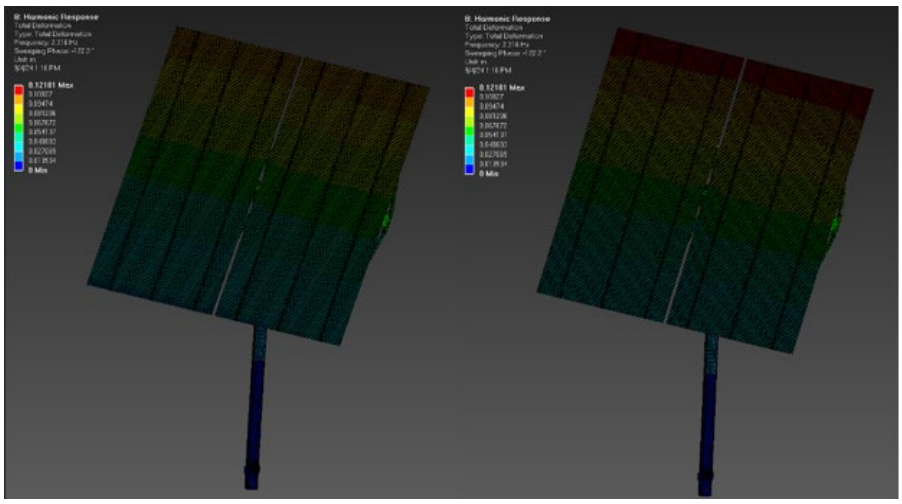

Figure 10. *S-Glass total deformation.*

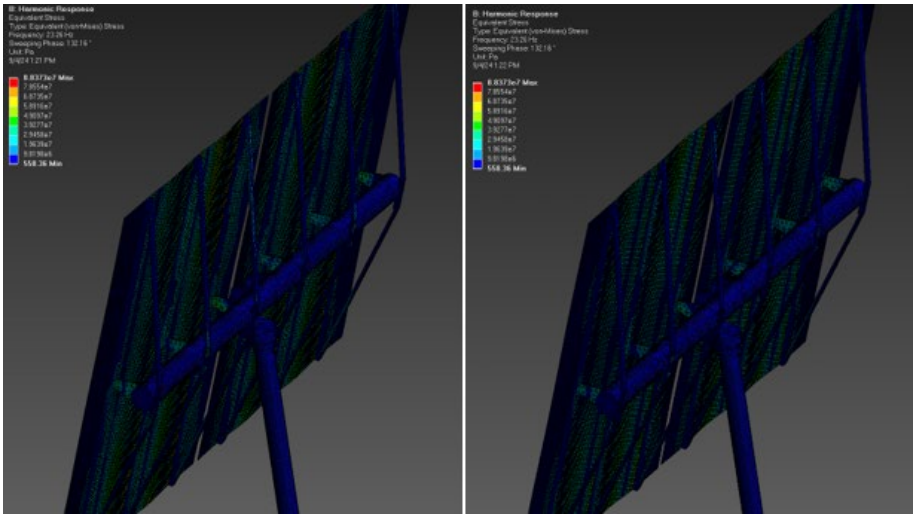

Figure 11. *S-Glass Von Misses stress.*

Figure 11 through 16 show the directional deformation and normal stress frequency response for the materials at 4, 8, and 16 m/s. Overall, the S-Glass shows the better response out of all the materials. It has the second lowest deformation behind steel and keeps the lowest stresses from all the materials.

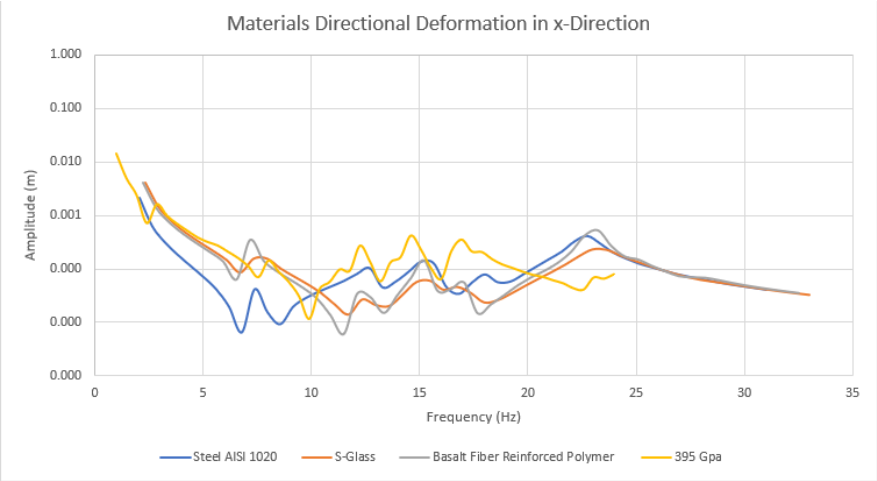

Figure 12. *Materials directional response at 4 m/s.*

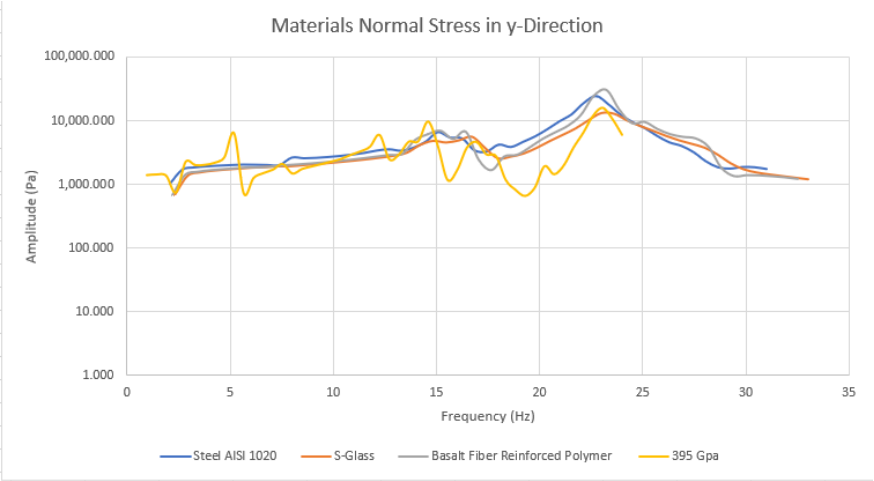

Figure 13. *Materials stress response at 4 m/s.*

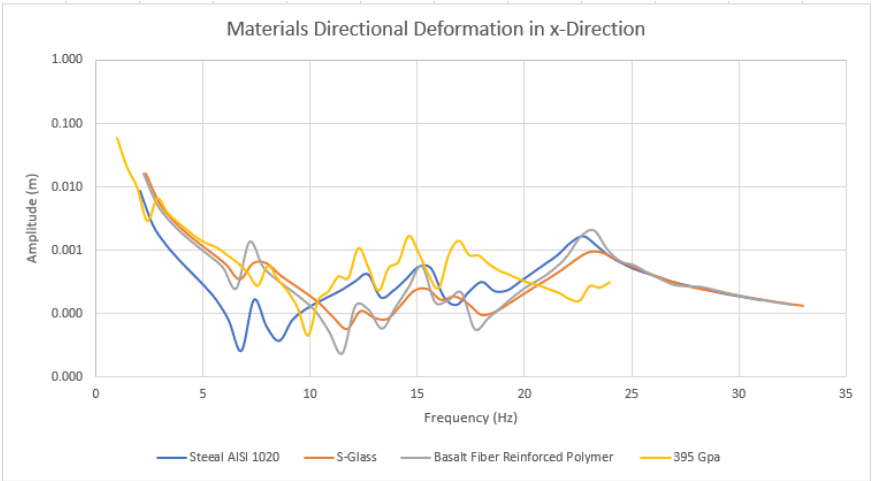

Figure 14. *Materials directional response at 8 m/s.*

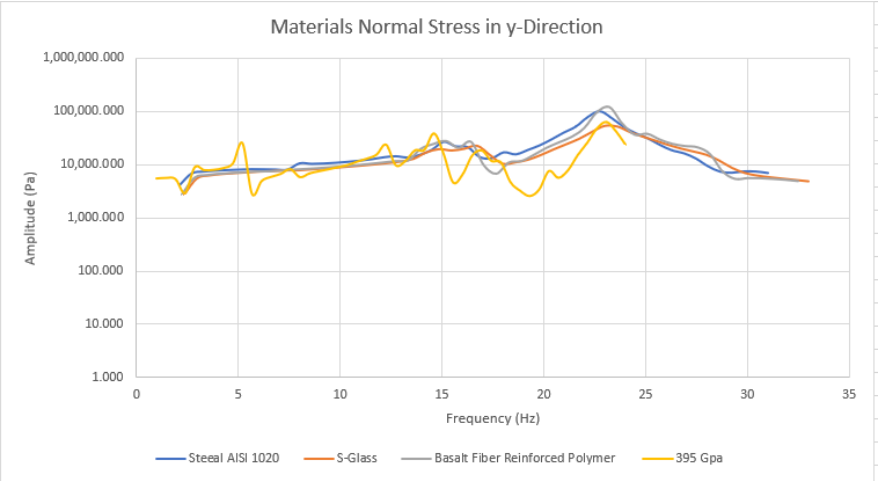

Figure 15. *Materials stress response at 8 m/s.*

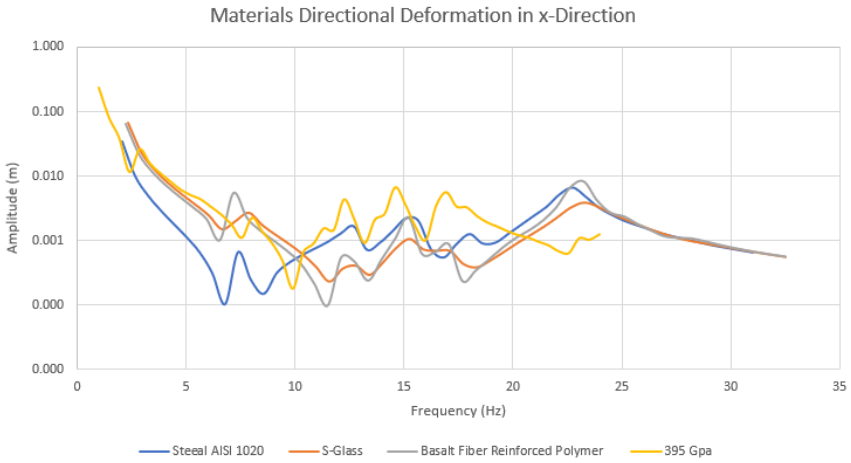

Figure 16. *Materials directional response at 16 m/s.*

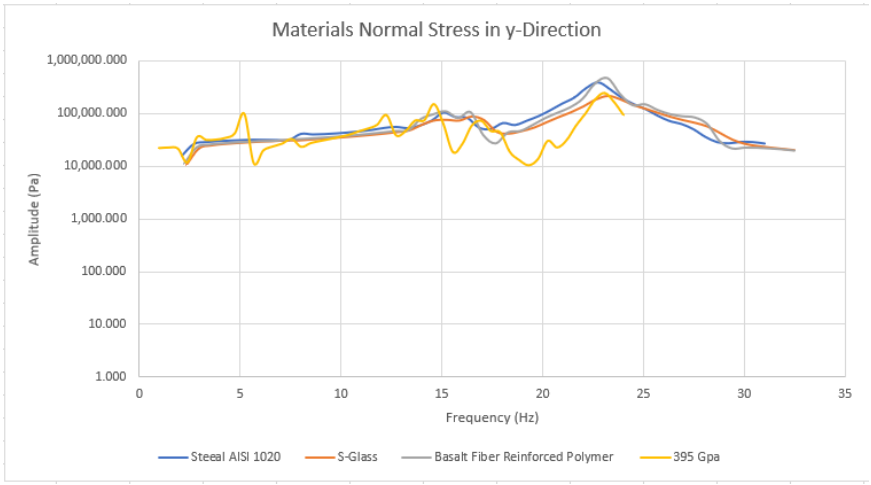

Figure 17. *Materials stress response at 16 m/s.*

4. Conclusions

The structural response of different manufacturing materials for heliostats at different wind speeds is presented. The load pressure from the wind was acquired through a CFD wind tunnel

study. The loads were imported into an FEA analysis where the natural frequencies and structural response was acquired. S-Glass and CF 395 showed great promise when comparing the max directional and normal stresses with the Steel AISI-1020. In all wind cases, the max normal stress was lower for S-Glass (0.013 – 0.21 MPa) and CF 395 (0.015 – 0.24 MPa) when compared to Steel ASIS-1020 (0.024 – 0.39 MPa). Steel AISI 1020 experienced the least amount of directional deformation at every wind case (0.0021 – 0.034 m), followed by S-Glass (0.004 – 0.065 m) and CF 395 (0.014 – 0.23 m). From all the materials, the S-Glass showed to have the best structural response. A testing campaign will now be conducted to validate these models.

Data availability statement

The data for this research work can be accessed directly from the authors.

Underlying and related material

Related materials can be obtained directly from the authors.

Author contributions

Javier Martell is credited with writing the manuscript, performing CFD simulations, and data analysis. Dimitri Madden is credited with project management, manuscript review, and data analysis. Kenneth Armijo is credited with project management and manuscript review.

Competing interests

The authors declare no competing interests.

Funding

Funding for this research was provided by the U.S. Department of Energy, Solar Energy Technologies Office (SETO).

Acknowledgement

Sandia National Laboratories is a multimission laboratory managed and operated by National Technology and Engineering Solutions of Sandia, LLC., a wholly owned subsidiary of Honeywell International, Inc., for the U.S. Department of Energy's National Nuclear Security Administration under contract DE-NA0003525.

References

[1] Kurup, P., Akar, S., Glynn, S., Augustine, C., & Davenport, P. (2022, February). Cost update: Commercial and advanced heliostat collectors. National Renewable Energy Laboratory. https://www.nrel.gov/docs/fy22osti/80482.pdf

[2] IEA (2024), CO2 Emissions in 2023, IEA, Paris https://www.iea.org/reports/co2-emissions-in-2023, Licence: CC BY 4.0

[3] Md Tasbirul Islam, Nazmul Huda, A.B. Abdullah, R. Saidur, A comprehensive review of state-of-the-art concentrating solar power (CSP) technologies: Current status and research trends, Renewable and Sustainable Energy Reviews, Volume 91, 2018, Pages 987-1018, ISSN 1364-0321, https://doi.org/10.1016/j.rser.2018.04.097.

[4] Weissert, J., Zhou, Y., You, D., and Metghalchi, H. (June 24, 2022). "Current Advancement of Heliostats." ASME. J. Energy Resour. Technol. December 2022; 144(12): 120801. https://doi.org/10.1115/1.4054738

[5] Todd Griffith, D., Moya, A. C., Ho, C. K., and Hunter, P. S. (October 23, 2014). "Structural Dynamics Testing and Analysis for Design Evaluation and Monitoring of Heliostats." ASME. J. Sol. Energy Eng. April 2015; 137(2): 021010. https://doi.org/10.1115/1.4028561

[6] Sathishkumar, G., R. Sridhar, S. Sivabalan, and S. J. Raja. 2019. Damping factor and dynamic mechanical analysis of glass fibre reinforced polyester composite. International Journal of Vehicle Structures & Systems 11, (3): 285-289, https://doi.org/10.4273/ijvss.11.3.13. https://www.proquest.com/scholarly-journals/damping-factor-dynamic-mechanical-analysis-glass/docview/2353052471/se-2 (accessed September 4, 2024).

[7] Zhang, B., Li, Z., Wu, H. et al. Research on damping performance and strength of the composite laminate. Sci Rep 11, 18281 (2021). https://doi.org/10.1038/s41598-021-97933-w

[8] Luyang Gong, Fengjia Zhang, Xiongqi Peng, Fabrizio Scarpa, Zhigao Huang, Guangming Tao, Hong-Yuan Liu, Helezi Zhou, Huamin Zhou, Improving the damping properties of carbon fiber reinforced polymer composites by interfacial sliding of oriented multilayer graphene oxide, Composites Science and Technology, Volume 224, 2022, 109309, ISSN 0266-3538, https://doi.org/10.1016/j.compscitech.2022.109309. (https://www.sciencedirect.com/science/article/pii/S0266353822000513)